buildings

MDPI

Article

Experimental Behavior of Existing RC Columns Strengthened with HPFRC Jacket under Concentric and Eccentric Compressive Load

Paolino Cassese [1], Costantino Menna [2,*], Antonio Occhiuzzi [1,3] and Domenico Asprone [2]

[1] Construction Technologies Institute (ITC)—Secondary Branch of Naples, National Research Council of Italy (CNR), c/o Polo Tecnologico di San Giovanni a Teduccio, 80146 Naples, Italy; paolino.cassese@itc.cnr.it (P.C.); occhiuzzi@itc.cnr.it (A.O.)
[2] Department of Structures for Engineering and Architecture, University of Naples Federico II, Via Claudio 21, 80125 Naples, Italy; d.asprone@unina.it
[3] Centro Direzionale—Isola C4, Department of Engineering, University of Naples "Parthenope", 80143 Naples, Italy
* Correspondence: costantino.menna@unina.it

Abstract: Reinforced concrete (RC) structures built before the 1970 represent a large portion of the existing European buildings stock. Their obsolescence in terms of design criteria, materials, and functionality is becoming a critical issue for guaranteeing adequate compliance with current structural codes. Recently, a new jacketing system based on the use of high-performance fiber-reinforced concrete (HPFRC) has been introduced for strengthening existing RC building members. Despite the promising aspects of the HPFRC jacketing technique, currently, a comprehensive and systematic technical framework for its implementation is still missing. In this paper, the experimental performance of RC columns strengthened with the HPFRC jacket subjected to pure axial load and combined axial load-bending moment uncoupled from shear is investigated. The test outcomes confirmed a significant improvement of the structural performance for the strengthened columns, especially for higher values of eccentricity. Finally, a standard-based practice-oriented analytical tool for designing retrofit interventions using the HPFRC jacket is proposed. The comparison between the calculated and experimental results revealed a satisfactory prediction capability.

Keywords: high-performance fiber-reinforced concrete; jacketing; experimental tests; axial load; retrofitting design

Citation: Cassese, P.; Menna, C.; Occhiuzzi, A.; Asprone, D. Experimental Behavior of Existing RC Columns Strengthened with HPFRC Jacket under Concentric and Eccentric Compressive Load. *Buildings* **2021**, *11*, 521. https://doi.org/10.3390/buildings11110521

Academic Editor: Francisco López Almansa

Received: 2 October 2021
Accepted: 3 November 2021
Published: 6 November 2021

1. Introduction

Reinforced concrete (RC) structures realized during the 1960s and 1970s represent a considerable portion of the existing building stock and their obsolescence in terms of design, materials, and functionality has become a critical issue in recent years [1,2]. These existing RC structures, generally designed in accordance with past design codes, may suffer severe damage as a consequence of the occurrence of seismic events due to insufficient shear or flexural strength or low ductility, resulting in premature failures [3–6]. In addition to such a dramatically well-known issue, the problem of durability, consisting in the degradation over time of initial/design mechanical properties, nowadays afflicts a large number of existing RC members [7,8].

Within such a framework, strengthening and repairing of RC members, particularly columns, is currently considered as one of the main challenges in the field of civil engineering. One of the most popular solutions is based on external jacketing of the existing RC structural element, which ensures considerable improvement of the mechanical performances, if well-designed [9]. Traditional external jackets are made of RC or steel, but several technical and practical inconveniences have been detected over time, such as an increase of the inertial mass of the whole structure or the difficulty in placing the supplementary steel

reinforcement [10,11]. Recently, lightweight and more manageable strengthening systems based on the use of fiber-reinforced polymers (FRPs) have been largely adopted in the field of seismic retrofit of existing RC members [12]. Nevertheless, they are characterized by significant limits in terms of fire resistance and reduced contribution to the lateral stiffness of structures [13,14].

During the last two decades, a new jacketing system based on the use of high-performance fiber-reinforced concrete (HPFRC) has been introduced for the strengthening of existing RC members, namely beams, columns, and beam-column joints ([15–20], among others), proving to be a valuable retrofit solution. Basically, a fiber-reinforced concrete (FRC) is a composite material made of concrete, which acts as matrix, and discontinuous short structural fibers (e.g., steel, carbon etc.) that are randomly mixed, which represent the intrinsic mechanical reinforcement. The concrete and fibers work together by means of the bond mechanism acting at the interface between the two different materials. In addition to a significantly improved compressive strength, FRC is typically classified in two different typologies, depending on its constitutive tensile response: strain-softening and strain-hardening. In the first case, cracking is strongly localized and tensile stress beyond the first cracking tends to reduce. Conversely, in the second case, cracks are distributed, and stress increases after the first cracking [21]. The FRC characterized by strain hardening is considered as "high-performance" (HPFRC) due to its improved ductility properties under traction loads. When applied as a jacketing system onto existing columns, the HPFRC is casted to enclose the existing RC member, the latter being deprived beforehand of the concrete cover. Such a system, from a mechanical point of view, enhances the properties of the strengthened RC members in terms of both the compressive and tensile strain/strength, mainly due to the limitation of cracks' openings because of the localized and so-called bridging effect activated by the steel fibers [22,23]. Furthermore, it has practical potential to avoid supplementary steel reinforcement installation, reduce the jacket thickness, and provide adequate fire resistance. Additionally, in terms of durability, HPFRCs (as an alternative to normal concrete) have demonstrated a remarkable ability to resist weathering conditions, chemical attack, and abrasion while maintaining their desired engineering properties [24]. This is related to a reduced number of voids of the HPFRC microstructure, which avoids the access of liquid or gas that could potentially activate degradation processes. Based on these beneficial aspects, recent studies reported that the HPFRC jacket is able to provide structural benefits to RC members regarding the load carrying capacity and energy dissipation, with a partial increase in lateral stiffness, hence improving the global structural performance of retrofitted buildings [18].

Currently, despite the above-reported promising aspects of HPFRC jacketing, a comprehensive and systematic technical framework is still missing, limiting its spread as a valuable retrofitting technique. Indeed, so far, either the experimental or numerical scientific literature appears to not be robust enough for its large-scale implementation, with relatively few test programs carried out [15–19,25–28] and rather complex numerical models proposed, which are mainly research oriented [29–32]. Furthermore, all the available research studies have investigated the flexure-shear capacity of HPFRC-strengthened RC members, under cyclic and monotonic loading, and none of them have dealt with the ultimate axial load capacity or bending uncoupled from shear. In addition, the main structural codes of practice [33–37] do not provide specific rules for the design of HPFRC jacketing of existing columns. Therefore, practitioners involved in seismic retrofitting may simply rely on only two design guidelines [38,39], which, however, are rigorously referred to in the design of structural members entirely made of FRC.

The present study aims to contribute to the above-mentioned research need and investigates the mechanical behavior of HPFRC-strengthened RC columns. Specifically, the study focuses on the structural performance under pure axial load and combined axial load-bending moment uncoupled from shear, and it is based on a specific experimental campaign. In the following sections, firstly, (i) the materials and specimens are described; then, (ii) the global and local experimental results are discussed along with the damage

states and failure modes; and finally, (iii) a standard-based practice-oriented analytical procedure is proposed and its effectiveness in predicting the recorded strength is discussed.

2. Experimental Program

A testing campaign was carried out at the Structural Laboratory of the Department of Structures for Engineering and Architecture at University of Naples Federico II aimed at the investigation of the mechanical behavior of HPFRC-strengthened RC columns. The following sections provide a detailed description of the specimens, materials, and experimental procedures adopted for the purpose of the study.

2.1. Description of Specimens

The experimental program was carried out on four reduced-scale specimens, one consisting in RC non-strengthened columns, assumed as the reference case, and three columns strengthened via external HPFRC jacketing. The overall specimen layout was conceived for the application of either axial load or combined axial load-bending moment uncoupled from shear. The non-strengthened RC columns were designed prior in order to be representative of typical Italian poor-detailed existing RC buildings in terms of both dimensions and reinforcement details [40]. Then, a scaling criterion equal to 1:2 was adopted, based on two considerations: (i) the attempt to study specimens whose dimensions were large enough to reproduce the behavior of real columns [41] and (ii) the need to respect laboratory constraints. The geometry and reinforcement details of the type-specimen are shown in Figure 1.

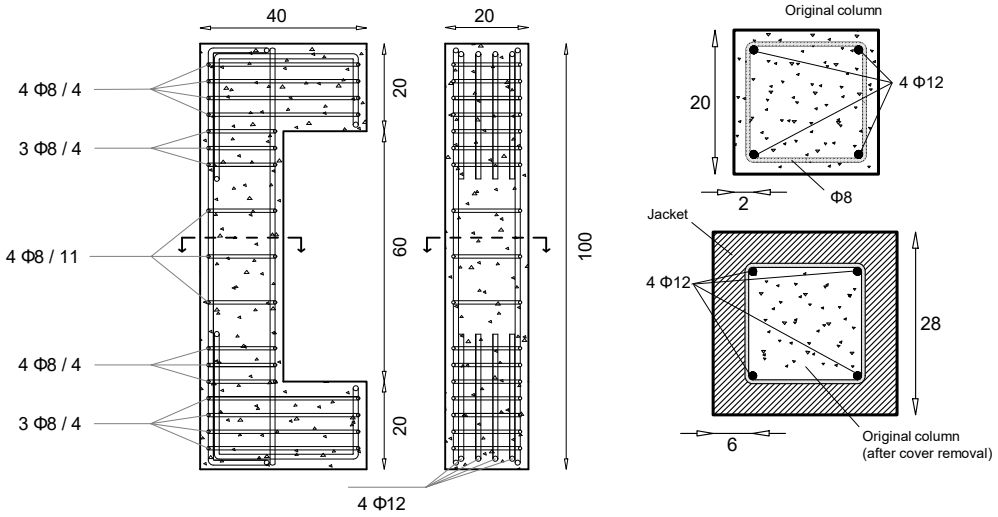

Figure 1. Geometry and reinforcement of the as-built specimens (**a**); details of the original and strengthened cross sections (**b**)—(dimensions in centimeters).

Half-scale reference (un-strengthened) RC specimens had a square cross-section of the side equal to 200 mm, with a 20 mm concrete cover and a total height of 1000 mm. The final span-to-depth ratio was therefore equal to 5.0. Steel reinforcement was composed of 4 Φ12 bars and Φ8 stirrups spaced at 110 mm in the central part of the column. The resulting reinforcement ratio values were 1.13% and 0.46%, respectively, in the longitudinal and transverse directions, within the typical range from the literature [42].

The as-built specimens were strengthened by applying a layer of HPFRC with a total thickness (t) of 60 mm to the RC reduced scale columns after the complete removal of the concrete cover from the existing concrete surface. This technique aimed to reproduce the removal of the concrete cover, which is necessary in the existing RC members due to environmental degradation/aging. The final square cross-section dimension (B = H)

was 280 mm. The columns' ends were characterized by properly designed corbels for the application of concentrated vertical loads at different eccentricities, resulting in more spatially dense stirrups (spaced at 40 mm). The HPFRC jacketing procedure consisted of different steps, as shown in Figure 2. After complete concrete cover removal (Figure 2a), the concrete surface was wetted to complete saturation and then a wooden formwork was constructed around the perimeter and along the full length of the column in order to allow fresh HPFRC pouring. Due to the self-compacting nature of the fresh mix, no vibration was needed to fully fill the gap between the formwork and inner concrete column. Given the high bond properties of the HPFRC material, no bonding agent or primer was employed at the HPFRC–inner concrete interface. Finally, HPFRC was manually poured into the formwork (Figure 2b,c), paying attention to uniformity and full filling, which was removed after the curing period of 14 days (Figure 2d).

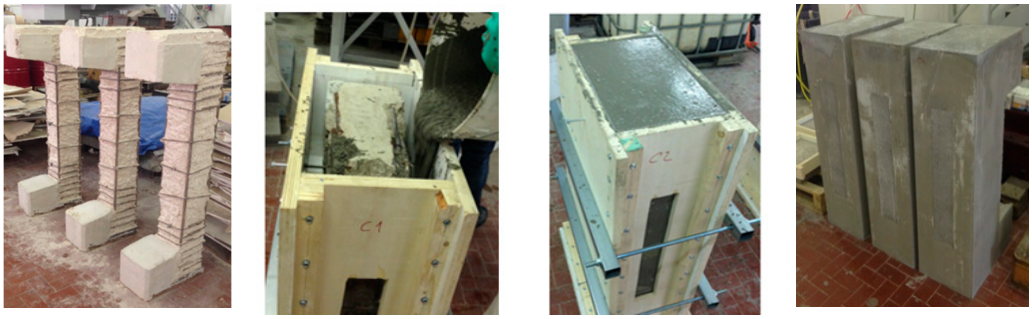

(**a**) (**b**) (**c**) (**d**)

Figure 2. Details of the HPFRC jacketing application to the as-built RC columns: concrete cover removal (**a**), fresh HPFRC pouring and curing (**b**,**c**), and the specimens after formwork removal (**d**).

2.2. Material Properties

For the external jacketing of the as-built specimens, an innovative HPFRC system was adopted. The relevant mechanical performances of the material adopted within the present experimental investigation allowed the traditional steel rebar reinforcement embedded in the jacketing layer to be avoided, in contrast to classical RC jacketing, which represents a crucial advantage for practical implementations. The HPFRC material was a self-leveling mortar characterized by a water/binder ratio of 0.34, with aggregates whose maximum size was equal to 4 mm and reinforced with 2.1% by volume of binder (V_f) of wavy steel micro-fibers, with a length of 18 mm and a diameter of 0.25 mm. The detailed composition in terms of the volume ratios with respect to the total binder is reported in Table 1.

Table 1. HPFRC composition in terms of the volumetric ratio with respect to the binder content.

Component	Volumetric Ratio (by Binder Content)
Water (w/c ratio)	0.340
Aggregates	1.750
Pozzolanic addition	0.032
SP admixture	0.010
SRA admixture	0.032
Steel fibers (V_f)	0.021

Compression tests were carried out on 12 cylindrical specimens (100 mm × 200 mm) according to the standard EN 12390-3 [43]. Tensile tests were performed on four notched specimens using an in-house direct tensile setup. The average compressive strength (f_c), after 28 days of curing, was equal to 121 MPa with a coefficient of variation (CoV) of 7%. The average tensile strength (f_t) was equal to 3.8 MPa with 4% CoV. Young's modulus (E_c) measured in both the compression and traction tests was equal to 37 GPa on

average. Figure 3 shows the averaged constitutive stress–strain (σ-ε) laws recorded under compression (Figure 3a) and tension (Figure 3b) regimes.

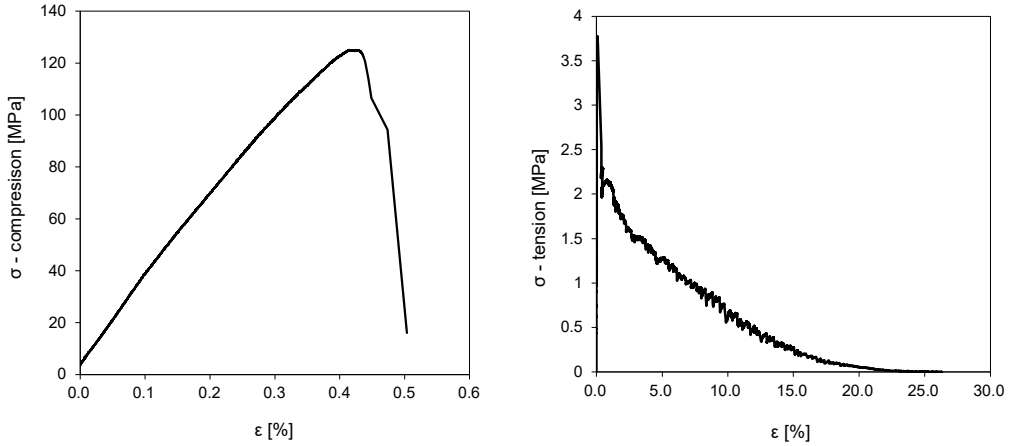

(**a**) (**b**)

Figure 3. Uniaxial compression (**a**) and tensile (**b**) average stress–strain diagrams of HPFRC material.

The adopted strengthening material reached very high compressive strength values; however, a very narrow post peak response was observed, with a pseudo-vertical drop to zero stress. On the contrary, the uniaxial tensile behavior was characterized by an almost linear softening phase up to 23% of the tensile strain, with a residual strength (after the peak) of about 2.1 MPa, which attributed a strain-softening behavior to the HPFRC material [44]. The main HPFRC mechanical properties and steel fiber dimensions are summarized in Table 2.

Table 2. Summary of the main properties of HPFRC *.

f_c ** (MPa)	f_t ** (MPa)	E_c ** (GPa)	Fiber Length (mm)	Fiber Diameter (mm)
121 [7%]	3.8 [4%]	37 [14%]	18 -	0.25 -

* Coefficient of Variation (CoV) given in square brackets. ** Average value on 6 samples.

As far as the RC columns are concerned, the non-strengthened specimens were built with poor concrete with a compressive strength ($f_{c,u}$), evaluated on six specimens according to EN 12390-3 [43], equal to 13 MPa on average, within the typical range of existing RC structures [45]. Steel reinforcement grade FeB450C [37] was used for both the longitudinal bars and stirrups. Standard tensile tests [46] were carried out on three steel specimens, revealing mean values of yielding strength (f_s) equal to 480 and 530 MPa, respectively, for diameters of Φ12 and Φ8, and elongation at maximum tensile force (A_{gt}) higher than 14%.

2.3. Testing Procedure, Set-Up, and Instrumentation

The main goal of the experimental campaign carried out in the present study was the assessment of the HPFRC jacked column performance under combined axial and bending load conditions uncoupled from shear. For this aim, a proper testing matrix was defined in which three different eccentricity values for the applied vertical load were investigated on three HPFRC-jacketed RC specimens (series S). The load-eccentricity (e) levels, kept constant during the tests, were identified based on the relative position of the loading point with respect to the kern depth (D_k) on the HPFRC-strengthened cross-section (see Figure 4). Accordingly, three different stress conditions were analyzed on the middle-span cross-section, as summarized in Table 3: (i) for e = 0 mm, pure compression was applied with a uniform distribution of the compressive stress; (ii) for e = 20 mm, a combined

axial load and bending regime was imposed with a fully compressed stress state; (iii) for e = 65 mm, a tension-compression stress state with a neutral axis that lay within the HPFRC jacketing layer (large eccentricity). In addition to the jacketed specimens, one unreinforced specimen (U1) was tested under pure compression as a reference case.

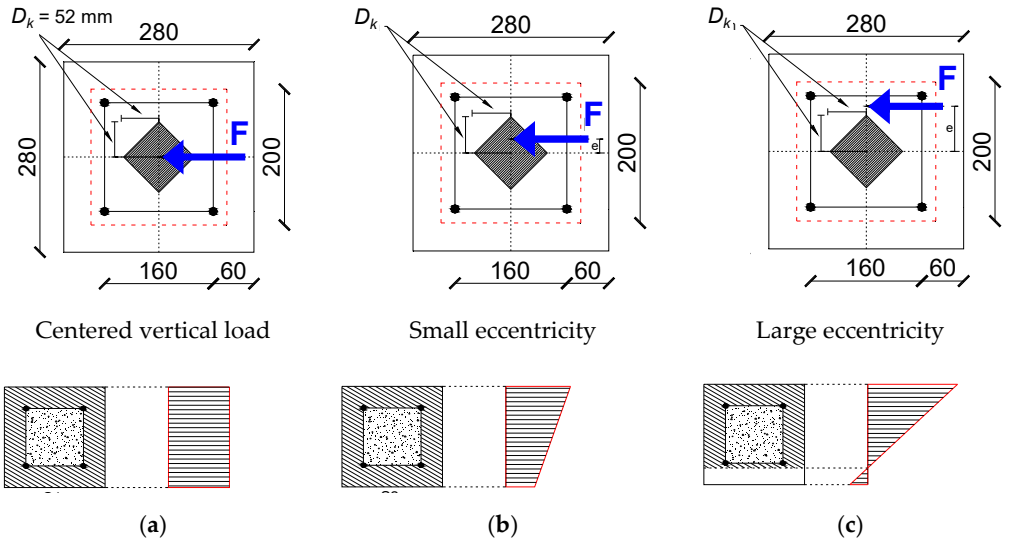

Figure 4. Loading configurations and corresponding stress states for specimens: S1, U1 (**a**); S2 (**b**); S3 (**c**) (dimensions in millimeters)—red dashed edges identify the existing column section.

Table 3. Scheme of the specimens and corresponding applied loading conditions.

Specimen	e (mm)	D_k (mm)	Stress Condition
U1	0	52	Pure compression (*Centered vertical load*)
S1	0		
S2	20		Combined bending and axial load (*Small eccentricity*)
S3	65		Combined bending and axial load (*Large eccentricity*)

A detailed scheme of the installed set-up and monitoring system is shown in Figure 5a. The conditions of combined axial-bending loading without shear and constant eccentricity with respect to the center of gravity of the column cross-section were obtained by means of two identical hinge devices, properly designed, applied to the specimen's ends. Specifically, two high-strength steel open cylindrical hinges were arranged to form the self-centering system shown in Figure 5b. Each system was made of an external female part fixed to the loading machine, and an internal male part fixed to the specimen's end. Between the hinge device and column, a 15 mm thick steel plate was placed in order to uniformly distribute the load and prevent local failures of the concrete cover due to the high compressive stress concentration.

Monotonically increasing load was applied under displacement control until failure, i.e., when major loss of the load-bearing capacity was recorded, with a rate of 0.002 mm/s to simulate quasi-static conditions. Since large load levels were expected, a high-performance servo-hydraulic machine Italsigma was used, which was able to reach up to 30,000 kN in compression.

All specimens were monitored with two couples of vertical linear variable displacement transducers (LVDTs) (namely, V1, V2, V3, V4) mounted on the opposite faces, measuring the average tensile and compressive strains, with a gauge length equal to 250 mm. In addition, local deformation of the HPFRC jacket was recorded by means of strain gauges placed at different levels of the column. The applied vertical displacement was measured by means of "LVDT Ext" connecting an external fixed reference and the moving crosshead to verify the displacement of the machine. A couple of vertical LVDT (namely, R1 and R2) were mounted at the basis of each specimen in order to assess the hinge rotation (α).

Finally, for the eccentric tests, the horizontal displacement of the middle span cross-section perpendicular to the specimen's axis was measured by a properly installed horizontal LVDT. The installed monitoring system is shown in Figure 5c.

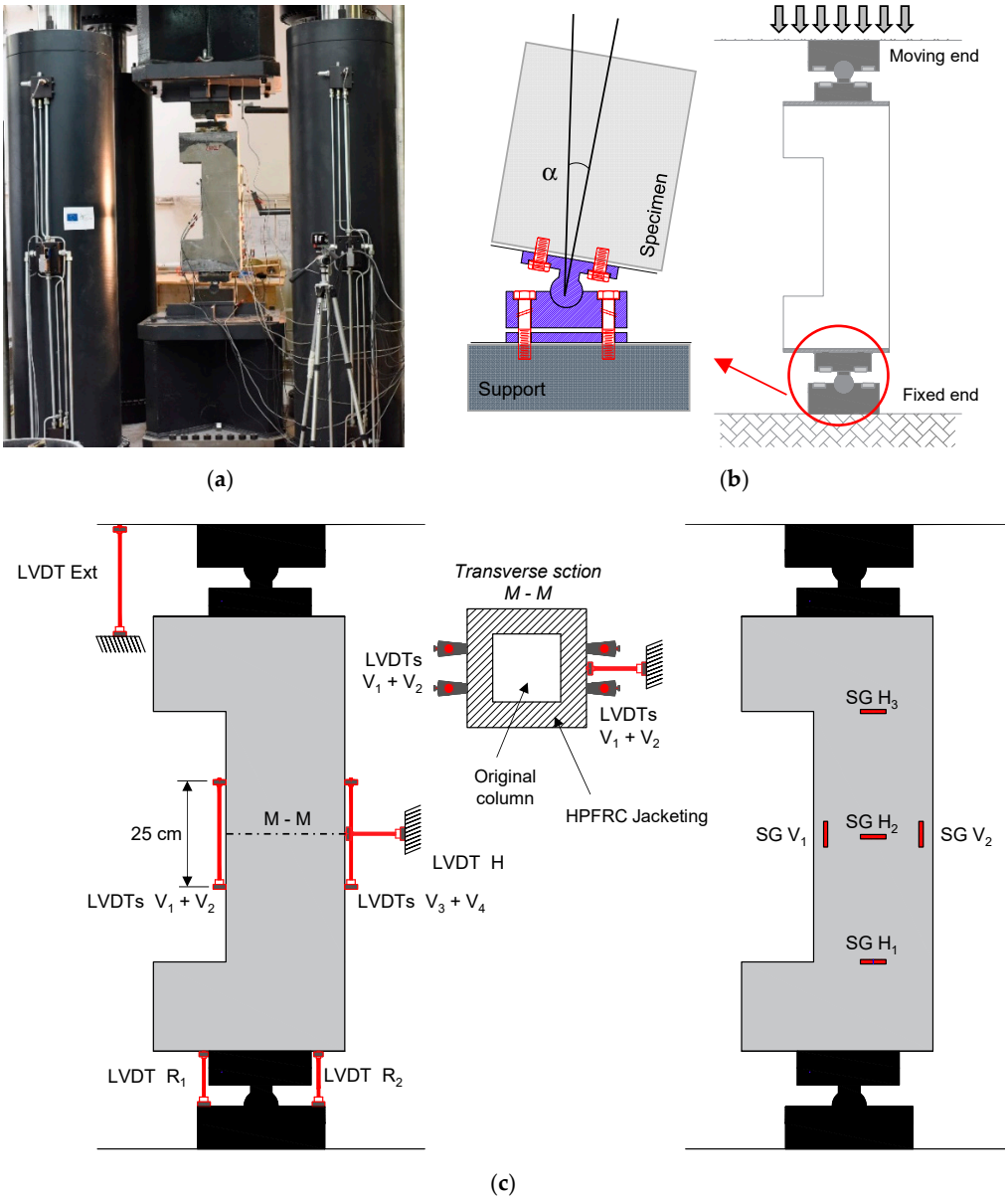

Figure 5. Experimental set-up and monitoring instrumentation: view of the specimen placed on the testing machine (**a**), and details of the adopted hinge system (**b**) and testing instrumentation scheme (**c**).

3. Results

Extensive testing outcomes in terms of both global and local measures were recorded via the above-described monitoring system along with the observed cracking evolution. The main experimental outcomes are described and analyzed in the following sections, first focusing on the numerical results, and then on the recorded damage states.

3.1. Mechanical Behavior

The recorded experimental response of either the reference RC or HPFRC jacketed columns is reported in terms of force vs. axial displacement (F-d) curves in Figure 6.

Specifically, Figure 6a shows the comparison between non-strengthened and jacketed specimens (i.e., U1 and S1) under pure compression load, whereas in Figure 6b, the effect of load eccentricity on the mechanical behavior is highlighted by means of the F-d curves of the strengthened columns S1, S2, and S3. The reported graphs are truncated, corresponding to a 20% strength reduction beyond the peak value, assumed as the conventional ultimate state, and the residual response is shown as a dashed line. The relevant response parameters are summarized in Table 4 in terms of the recorded axial load peak (F_{max}), displacement in the peak (d_p) and ultimate (d_u) conditions, axial stiffness (K_p) (assumed as secant at the peak) and dissipated energy (E_d), given as the area underneath the F-d curves up to the 20% strength drop.

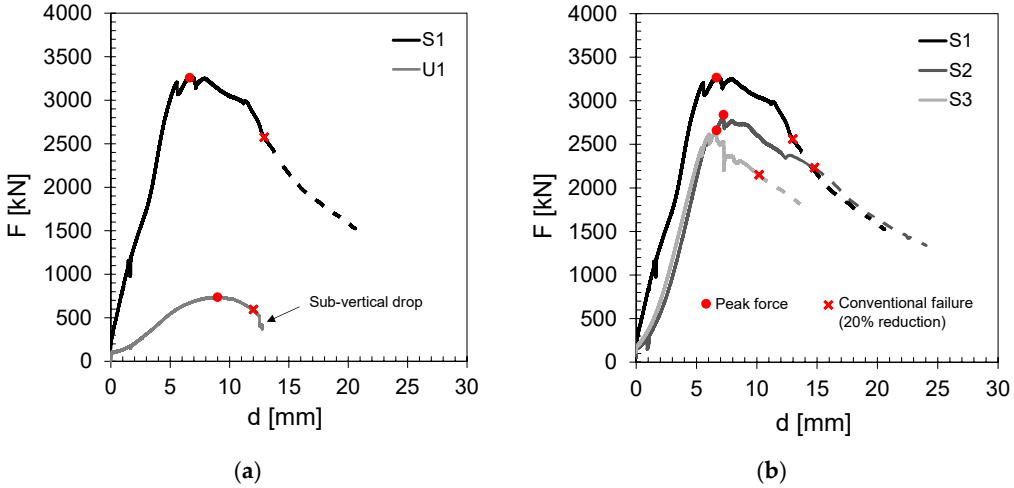

Figure 6. Axial load vs. displacement (F-d) diagrams for specimens: U1–S1 (**a**); S1–S2–S3 (**b**).

Table 4. Main recorded experimental parameters.

Specimen	F_{max} (kN)	d_p (mm)	d_u (mm)	K_p (kN/mm)	E_d (kNmm)	g_f (-)
U1	737	8.9	12.1	82.8	4000	-
S1	3265	6.8	12.8	480.1	46,900	4.4
S2	2818	7.1	14.8	396.9	45,700	4.8
S3	2652	6.6	10.3	401.8	25,300	6.5

The control non-strengthened specimen U1, tested in the pure compression regime, showed an initial pseudo-linear elastic branch followed by a pronounced non-linear part starting from 500 kN, with a gradual reduction of the stiffness corresponding to cracking evolution up to the load peak (F_{max}) value equal to 737 kN and 8.9 mm displacement at the peak (d_p). Beyond the peak, a steep softening was recorded until failure was reached, with a sub-vertical drop in strength corresponding to a displacement of 12.2 mm due to the combination of steel reinforcement buckling and concrete crushing occurring at similar strain levels of about 0.2%. A substantially higher compressive strength value was reached, as expected, by the HPFRC jacketed specimen S1 (under the same load condition, i.e., pure compression), equal to 3265 kN corresponding to a displacement value of 6.8 mm, lower than the non-strengthened column. The F-d curve was characterized by a first elastic branch until the 3200 kN load was reached. Then, a sudden drop of the stiffness was observed, corresponding to the cracking occurrence in the HPFRC external part, and, subsequently, the peak load was reached. The mechanical post-peak response developed along a gradual softening branch until the inner original concrete core was completely crushed. Then, a steeper reduction of the bearing capacity was detected since the fiber bridging action was no longer effective due to the wider crack openings. By comparing the results of such specimens (i.e., U1 and S1), it is worth noting that the strengthened

column showed a very improved performance in terms of both the strength and stiffness, with an increase equal to approximately 4.4 and 5.8 times, respectively, compared to the as-built RC member. As confirmation, by computing the energy (E_d) dissipated by the specimens U1 and S1, the latter dissipated an amount of energy almost 10 times greater than the non-strengthened one (4000 J against 46,900 J).

The experimental F-d diagrams of the specimens S2 and S3, tested under combined axial and bending loads (e = 20 mm and e = 65 mm, respectively), were characterized by a similar trend with respect to specimen S1, except the sudden drop of the post-peak softening slope. In fact, a gradual softening branch was observed until complete failure of the specimens occurred. For specimens S2 and S3, a reduction of the strength performance was recorded with respect to the simply compressed specimen S1 due to the different stress/strain distribution induced on the cross-section. In fact, load peak values equal to 2818 and 2652 kN were reached for the S2 and S3 specimens, respectively, whereas almost similar values of axial displacement at the peak were recorded, specifically 7.1- and 6.6-mm. Dissipated energy (E_d) values equal to 45,700 and 25,300 J for specimens S2 and S3 revealed a considerable reduction in the dissipation capacity when the cross-section was not fully compressed (i.e., with load eccentricity e = 20 mm).

In order to assess the efficiency of the HPFRC jacketing technique in comparison with the RC (as-built) specimen, firstly, the axial force–bending moment (P-M) interaction diagram was computed for the non-strengthened specimen. Then, the P-M values were determined analytically for the jacketed columns. Finally, the P-M values derived for the eccentricities of interest (i.e., e = 20 mm and e = 65 mm) were compared with the corresponding experimental outcomes. Such a hybrid comparison was due to the sake of convenience in order to avoid testing the well-known response of the as-built RC members for which P-M curve validation is broadly recognized [47].

The P-M domain of the non-strengthened column was computed under the classic RC simplified assumptions, including the ultimate limit state of planarity of the cross-sections, tensile strength of the concrete equal to zero, and a perfect steel-concrete bond. As constitutive laws of the materials, standard-based models of stress-block and elastic-plastic envelopes were assumed for concrete and steel, respectively [33]. The outcomes are graphically reported in Figure 7a for the positive quadrant of the P-M domain. Notice that the experimental axial capacity (F_{max}) of the specimen U1 was numerically predicted with negligible approximation (error equal to 0.9%, with 744 kN predicted vs. 737 kN recorded). By assuming that the three experimental points (P-M) lie on a HPFRC strengthening envelope, the strength improvement of the column subjected to eccentric compressive load was determined in terms of the gain factor (g_f), computed according to Equation (1), the meaning of which is schematically depicted in Figure 7b. In Equation (1), the coordinates (P_{Ui}, M_{Ui}) and (P_{Si}, M_{Si}) are given by the axial load and ultimate bending moment values of the non-strengthened and strengthened columns, respectively, characterized by the same eccentricity. The g_f values are summarized in Table 4.

$$g_f = \sqrt{\frac{(P_{Si} + M_{Si})^2}{(P_{Ui} + M_{Ui})^2}} \quad (1)$$

The g_f values obtained for specimens S2 and S3, respectively, were equal to 4.8 and 6.5, which are larger with respect to the pure compression case (i.e., specimen S1). Such experimental findings, namely the improvement of the mechanical performances (i.e., strength, stiffness, and dissipated energy), were consistent with the strengthening system typology. In fact, the external HPFRC layer was characterized by high compression strength and bridging action of the steel fibers in the presence of tensile stress. Furthermore, the HPFRC jacket delayed the activation of the failure mechanism of the non-strengthened columns, characterized by the combination of compressive steel bar buckling and concrete crushing.

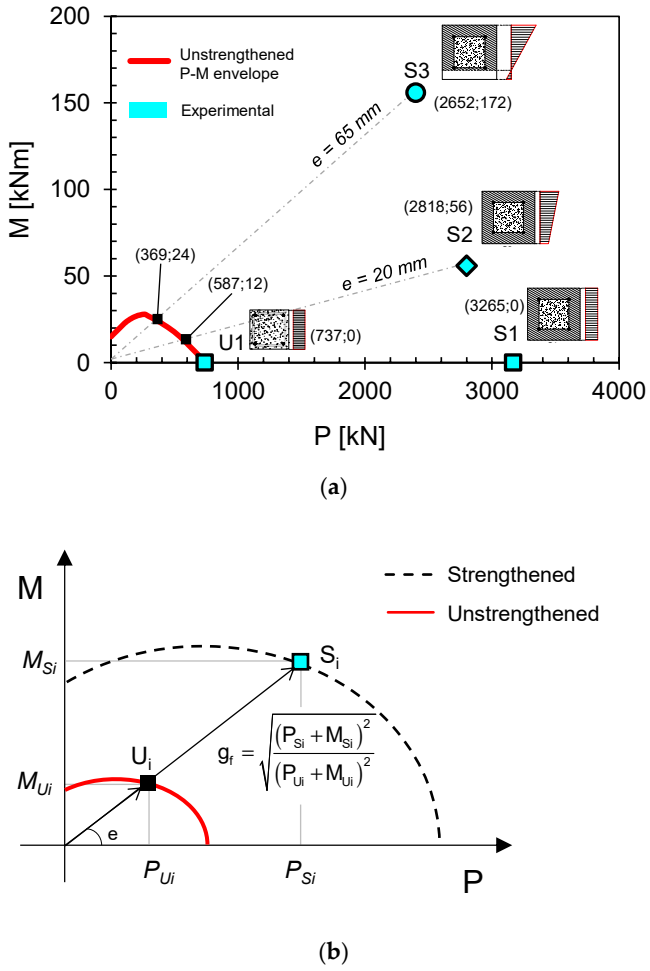

Figure 7. Axial force–bending moment (P-M) diagram (**a**) and gain factor definition (**b**).

3.2. Damage and Failure Modes

In light of the mechanical response described in detail in the previous section, a report focused on the specimens' damage evolution and failure modes is presented herein. The non-strengthened specimen U1 failed because of the combination of steel reinforcement buckling and concrete crushing. The damage state was characterized by pseudo-vertical cracks appearing on the external surface of the specimen starting from about the 500 kN load. The cracks' width increased with the applied displacement, particularly in the central part of the specimen, where the concrete cover firstly spalled-out. Severe crushing of the concrete core was observed in the peak load condition. Damage dramatically evolved until ultimate failure occurred at a compressive strain level higher than 0.29%, when the vertical displacement reached 12.1 mm. The final damage state for specimen U1 is reported in Figure 8a.

The failure mode of all HPFRC strengthened columns, tested either under uniaxial or eccentric load, was similar and due to the compressive failure of the HPFRC layer. The damage state evolution developed in a distinct fashion among the S-specimens. For the column S1, the first cracks appeared on the external surface for a vertical load of about 3100 kN. These cracks were mainly located toward the member's ends, in contrast with the specimen U1, due to local interaction phenomena triggered by the transverse expansion of the concrete core. Subsequently, these cracks suddenly increased their width, and the peak load condition was reached. Then, during the post-peak phase, the principal vertical crack developed at the base of the specimen along the lateral core–jacket interface, and critically enlarged until the failure condition was reached, corresponding to a vertical displacement of 12.8 mm. A detailed view of the base crack is shown in Figure 8b.

(**a**) (**b**)

Figure 8. General views (frontal or lateral) and details of the final damage states for the specimen U1 (**a**) and S1 (**b**).

Specimen S2 showed a damage evolution very similar to the previous one. Indeed, also in this case, the first noticeable vertical cracks appeared for load values close to the peak, specifically about 2700 kN, on both the side surface and on the more compressed edge of the columns. The softening branch was mainly governed by the gradual opening of the main crack located next to the top end of the specimen, whose detail is reported in Figure 9a. Such a crack also intersected the corbel, which resulted in damage at the end of the test. Specific damage development was observed for the specimen S3 (see Figure 9b), subjected to vertical load in a large eccentricity value. As confirmed by the longitudinal LVDT measurements of the HPFRC surfaces under tension and compression, the neutral axis in this case was found to be within the cross-section. Therefore, the resulting tension-compression stress state produced horizontal tensile cracks within the HPFRC layer that developed in an almost regular manner (see crack paths highlighted in red in the figure) along the overall length of the column. These cracks were approximately 2 mm wide (onto the external surface) in correspondence with the peak load.

(**a**) (**b**)

Figure 9. General views (back or lateral) and details of the final damage states for the specimen S2 (**a**) and S3 (**b**).

One of the aspects that is investigated regarding the damage state of the core-jacket system is related to potential slip between the two components. Unfortunately, such analysis could not be performed by immediate visual inspection because the bond was well preserved even after major damage, as can be observed from a representative interface piece that was removed from the column (post-mortem) and is shown in Figure 10. Therefore, for one of the tests carried out, specifically for specimen S2, thermal imaging was carried out, with the aim of identifying any crack along the core/jacket surface. Figure 11 shows the details of two thermographic images captured on the internal and external compressed sides. The thermography did not reveal any internal slip. Indeed, only cracks on the

external jacket surface were confirmed; therefore, no debonding between the HPFRC jacketing layer and inner RC was detected.

Figure 10. Detailed image of a representative interface piece removed from specimen S2.

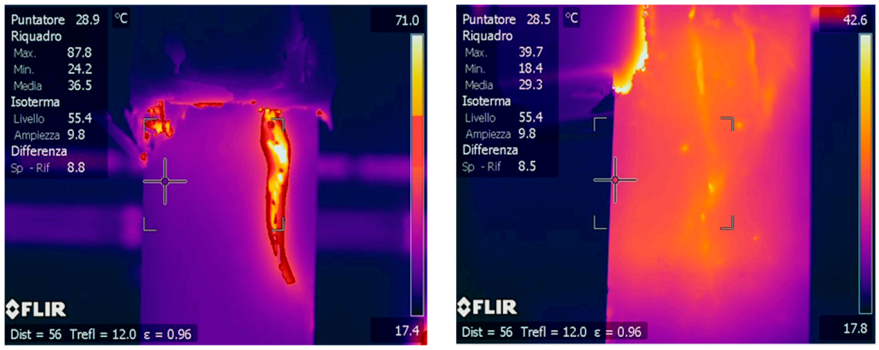

(**a**) (**b**)

Figure 11. Thermographic images of the internal (**a**) and external (**b**) compressed edges of specimen S2.

3.3. Local-to-Global Response

The deformation measured by the local monitoring LVDT system described in Section 2.3 was analyzed, aiming to deeply investigate the effect of the HPFRC jacket on the mechanical response of the RC specimens. The longitudinal (axial) deformation (ε_1) of each specimen was computed as the average value recorded by the vertical LVDTs (V1–V4) normalized to the initial base-length (equal to 25 cm).

With reference to the specimens U1 and S1, the non-strengthened and jacketed columns tested under pure compressive loading force versus longitudinal deformation (F-ε_1) curves are shown in Figure 12. Plots are reported until deformation measures from LVDTs can be considered reliable, namely until loss of instrumentation occurred due to damage development. Accordingly, for the specimen U1, the F-ε_1 curve is arrested in the incipient peak load condition, whereas, for the specimen S1, LVDTs were lost shortly beyond the peak load. Figure 12 shows that the maximum recorded force was reached by the specimen U1 at an ε_1 slightly larger than 0.29%. Conversely, the peak load was achieved by the strengthened column U1 for a value deformation equal to 0.17%, which was considerably lower. Such a finding suggests that under compressive axial load, if large compressive strains are internally reached, the interaction between the concrete core and the HPFRC jacket cannot be considered as fully effective.

This is confirmed by the theoretical prediction of the compression capacity. Indeed, by assuming a uniform response of the cross-section among the two materials, i.e., both RC and HPFRC fully effective, the predicted compression strength ($F_{max,t}$) can be simply computed according to Equation (2), where $A_{c,u}$ and A_c are the unreinforced and HPFRC cross-section areas, and $f_{c,u}$ and f_c are the core concrete and HPFRC compressive strength

values, respectively (given in Section 2.2). Notice that for the sake of convenience, the contribution of steel bars in the core was neglected:

$$F_{max,t} = f_{c,u}A_{c,u} + f_cA_c \quad (2)$$

The value of $F_{max,t}$ provided by Equation (2) is equal to 6721.6 kN, approximately twice the recorded peak load Fmax. The observed reduced performance of the HPFRC jacketed columns with respect to the theoretically predicted value (in terms of the compressive strength capacity) was due to the inaccurate assumption of the simple analytical model considered. In fact, due to vertical compression loading and for larger compression strains, the inner concrete core is subjected to considerable transverse expansion, which is constrained by the HPFRC jacket layer. Particularly, when the overall longitudinal deformation (ε_l) of the original core reached values larger than 0.15%, the concrete was severely cracked and showed spalling-out due to non-linear deformations. As a result, the external jacket was subjected to a biaxial stress state characterized by transverse (σ_t) stress in addition to longitudinal compressive stress (σ_l), causing tension in the outer portion and, therefore, early cracking once tensile strength was reached. In Figure 13, such a phenomenon is schematically depicted with reference to the half part of a HPFRC elementary block, with reference to the pure compression load case.

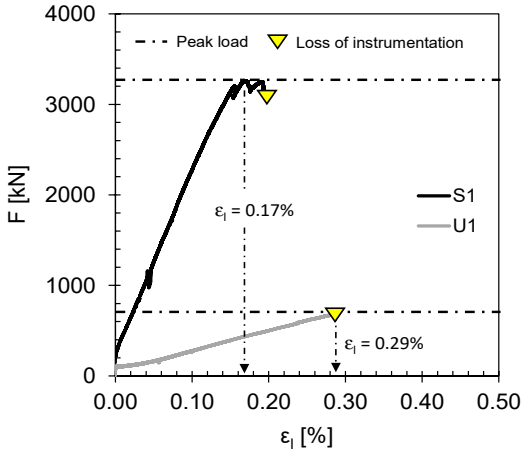

Figure 12. Load–longitudinal deformation (F-ε_l) diagram for the specimens U1 and S1 tested under pure compressive load.

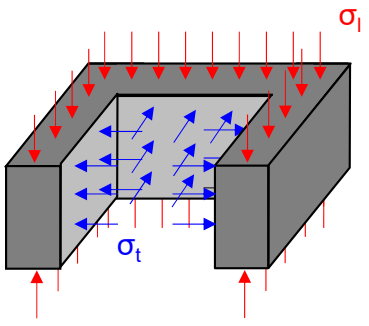

Figure 13. Schematic view of the stress state on the half part of a HPFRC elementary block of the specimen S1.

A further confirmation of such a phenomenon is given by the results related to the jacketed specimens S2 and S3 subjected to the eccentric compressive load given in Figure 14 in terms of the longitudinal concrete strain versus the vertical displacement (ε_l-d). In these cases, the strain ε_l was obtained as the average measure recorded by the LVDTs installed

on the more compressed edge of the cross-section (namely, V3–V4) and the plots are again reported until the deformation measures from LVDTs can be considered reliable.

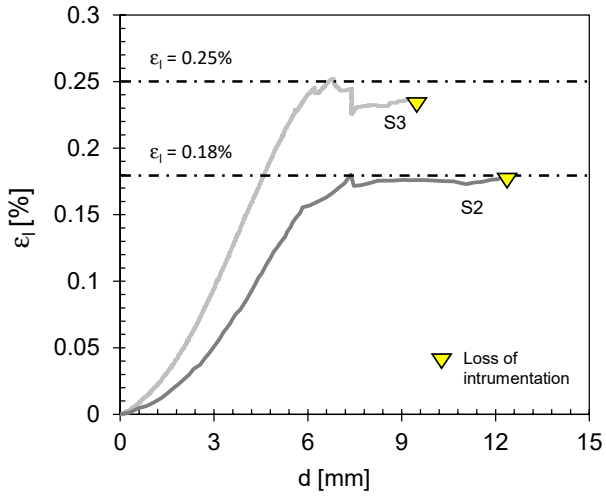

Figure 14. Longitudinal deformation vs. global displacement (ε_l-d) for the specimens S2 and S3 tested under the eccentric compressive load.

For the specimen S2, the strain ε_l increased with the applied displacement until a value of 0.18% was reached on the more compressed edge at about 7 mm of shortening (d), close to the peak load condition, when severe damage was observed. Beyond such a displacement, this value was kept constant until the monitoring instrumentation was interrupted due to the major cracks becoming wider. Conversely, higher maximum strain ε_l was measured for the specimen S3, which was equal to 0.25%, corresponding to a global displacement of about 6.5 mm, namely in the peak load condition. Subsequently, a drop of ε_l was observed, probably due to stress/strain redistribution. These results are in agreement with the proposed interpretation model, according to which the influence of transverse stress on the HPFRC strengthening performance depends on the level of compression experienced over the resisting area generated by a given load value. Thus, the transverse stress (σ_t) associated with the inner concrete expansion and the subsequent transverse dilatation of the concrete is less significant for the specimen S3 for which, due to the higher eccentricity of the applied load, the compression level and the depth of the compressed zone on the cross-section are lower. On the contrary, for the specimen S2, an intermediate case (between S1 and S3) in terms of the compressed area is reached.

4. Analytical Interpretation

As already mentioned in the Introduction section of this paper, currently, a practitioner working on the design of a retrofit intervention by means of HPFRC jacketing of existing RC columns cannot rely on specific provisions given by the main structural standards. As a matter of fact, with particular reference to the case of interest of the combined axial load and bending moment, specific design formulations and instructions are available within only two technical guidelines [38,39]; however, these are relevant only for the design of (whole) normal or high-performance fiber-reinforced concrete (FRC) members. Therefore, no specific formulation for the use of HPFRC as a jacketing system of existing RC members is suggested, despite several research studies highlighting distinctive issues potentially affecting the failure modes, and thus the ultimate capacity of HPFRC strengthened members (such as the debonding at the jacket/core interface) [19]. In this regard, a specific simplified analytical approach for determining axial force–bending moment (P-M) capacity diagrams is herein proposed. The prediction effectiveness is assessed by analytical-to-experimental strength comparison.

The CNR and FIB technical guidelines for the design of full-FRC members [38,39], i.e., structural elements entirely made of FRC, suggest very similar approaches for the ultimate limit state (ULS) verification under combined axial force–bending moment (P-M). Accordingly, the fundamental hypotheses at ULS are: (i) plane sections remain in plane (yielding linear strain distribution) and (ii) there is a perfect bond between the rebars and the surrounding FRC. For the jacketing case investigated in this study, a perfect bond is assumed at the core–jacket interface, since such a condition is obtained by means of a proper connection characterized by high superficial roughness [48]. The simplified approach is based on the evaluation of internal forces starting from the stress distribution on the cross-section through equilibrium equations. Therefore, constitutive laws of all the constituent materials are needed. As reported in the CNR guideline [38], the compressive behavior of FRC can be assumed to be equal to that of ordinary concrete of a high strength class since, in the cases investigated, the presence of fibers does not have a significant effect on the overall shape of the constitutive (σ-ε) diagram; thus, in accordance with the Eurocode 2 [33], a simplified rectangular stress–strain (σ-ε) relationship at ULS is adopted (stress-block) at failure for both the compressed core and jacket concrete of cross-sections subjected to bending moment. Moreover, due to the absence of steel reinforcement in the FRC jacket and the very low transverse reinforcement amount in the concrete core, no confinement effect on the latter is assumed [49]. A symmetric elastic perfectly plastic relationship is assigned to core steel bars [33].

As for the tensile σ-ε response of HPFRC, experimental evidence shows that it generally consists of: (i) a first ascending elastic branch until the first crack forms, (ii) a sudden strength drop, and (iii) a third softening phase until zero stress is reached for large axial strain (ε) values, typically higher than 0.04, which correspond to complete fiber pull-out from the concrete matrix. Accordingly, several multi-linear constitutive laws are available for FRC in the literature [23,50–53], but these models are strongly dependent on the empirical results on which they are based. Herein, in order to develop a practice-oriented code-based procedure, the elastic-plastic material model suggested by the CNR guideline [38] is applied (see Figure 15).

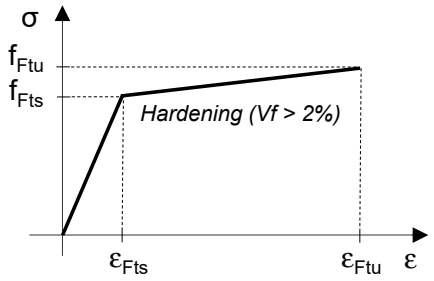

Figure 15. Constitutive law for FRC in tension (adapted from [38]).

Such a model requires the execution of the standard bending tests established in [54] to determine the serviceability (f_{Fts}) and ultimate (f_{Ftu}) residual strength values according to Equations (3) and (4), wherein, f_{eq1} and f_{eq2} are the post-cracking equivalent strength in the service and ultimate conditions, respectively; and w_u and w_{i2} are the ultimate crack opening and the mean crack width corresponding to f_{eq2}. The serviceability (ε_{Fts}) and ultimate (ε_{Ftu}) deformation limits are assumed to be equal to 0.15% and 1% [23,38]. In tune with the fiber content (V_f), a slight hardening characterizes the flexure-induced tensile behavior of the adopted HPFRC material. Accordingly, f_{Fts} and f_{Ftu} are equal to 6.0 and 9.3 MPa, respectively:

$$f_{Fts} = 0.45 f_{eq1} \tag{3}$$

$$f_{Ftu} = f_{Fts} - \frac{w_u}{w_{i2}} \cdot \left(f_{Fts} - 0.5 f_{eq2} + 0.2 f_{eq1}\right) \geq 0 \tag{4}$$

Designed P-M curves may be obtained according to a simplified approach based on the definition of notable failure conditions generated by specific loading conditions applied to the strengthened RC column. From these conditions, the corresponding P-M values are computed starting from the assumed strain distributions (derived from the corresponding constitutive laws of each component of the cross-section). Finally, the points of the coordinates (P, M) are fitted to obtain a resisting domain associated with the structural element considered. In this regard, and as a classical approach for normal concrete in structural engineering, we preliminarily assume that the failure of the HPFRC jacketed column subjected to axial and/or bending loads may be attributed to two distinct phenomena: (i) attainment of the maximum compressive strain (ε_{cu}) in the HPFRC jacket, and (ii) attainment of the maximum tensile strain (ε_{sy}) in the steel rebars. Therefore, different strain distributions at failure can be derived as schematically depicted in Figure 16.

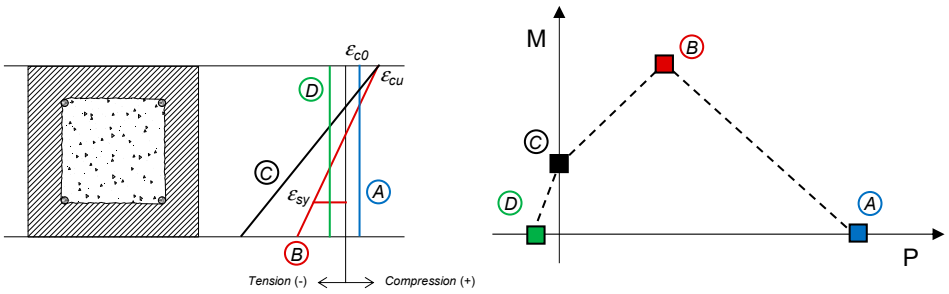

Figure 16. Strain distribution at failure for determining the P-M interaction domain.

Pure compression failure (condition A) occurs when the axial load (P_A) is such that the concrete core, jacket, and steel reinforcement reach their ultimate compressive strength, according to Equation (5), wherein, $A_{s,uc}$ is the total cross-sectional area of the steel bars in the concrete core, whereas all the remaining symbols were previously defined. Longitudinal compressive deformation (ε_{c0}) is uniformly distributed over the cross-section and is equal to 0.2% [33]:

$$P_A = f_{u,c}(A_{u,c} - A_{s,uc}) + f_c A_c + A_{s,uc} f_s \quad (5)$$

The so-called balanced failure (condition B) is obtained when simultaneously tensile steel yields and compressed HPFRC crushes. Accordingly, a linear strain distribution is assumed on the cross-section identified by: (i) the ultimate value of the compressive strain (ε_{cu}) at the most compressed edge for the HPFRC and (ii) the yielding strain (ε_{sy}) in the tensile steel longitudinal bars. Therefore, with reference to Figure 17, the neutral axis depth (x_B) is simply derived from linearity considerations through Equation (6), wherein the ultimate value of the HPFRC compressive strain (ε_{cu}) is assumed to be equal to 0.35% [33] and the steel yielding strain is 0.21% (ε_{sy}):

$$x_B = \frac{\varepsilon_{cu}}{\varepsilon_{cu} + \varepsilon_{sy}}(H - t) \quad (6)$$

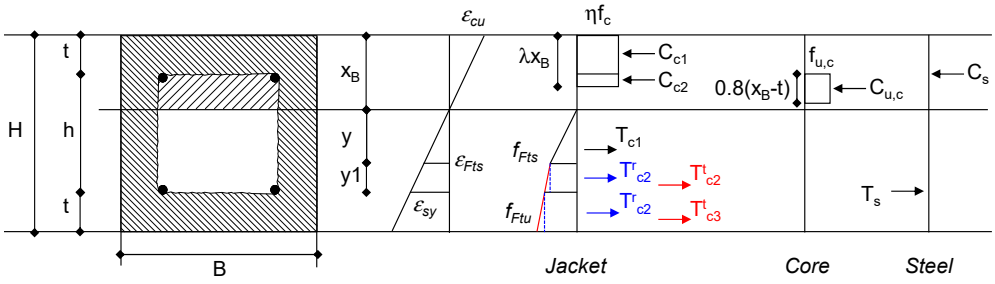

Figure 17. Equilibrium of the internal forces acting on the cross-section (balanced failure).

At this point, assuming the strain and stress distributions shown in Figure 17, the internal forces can be simply evaluated. Then, the axial load (P) is obtained from the longitudinal forces equilibrium equation reported in Equation (7) and the corresponding bending moment (M) as a result of the equilibrium to rotation about the *x*-axis by Equation (8). In Equations (7) and (8), the stress-block coefficients λ and η are computed according to Eurocode 2 [33], whereas the terms y and y_1 are derived through triangle similarity starting from the deformation distribution (see Figure 17):

$$P = C_{c1} + C_{c2} + C_{u,c} + C_s - T_{c1} - T_{c2} - T_{c3} - T_s \quad (7)$$

$$\begin{aligned} M = {} & C_{c1}(x_B - t/2) + C_{c2}(x_B - \lambda x_B/2 - t/2) + C_{u,c}(x_B - t - \lambda x_B/2) + C_s(x_B - t) - T_{c1}(2/3y) + \\ & + T^r_{c2}(y + y_1/2) + T^t_{c2}(y + 2/3y_1) + T^r_{c3}(H - x_B - t/2) + T^t_{c3}(H - x_B - 1/3t) + T_s(H - t - x_B) \end{aligned} \quad (8)$$

The pure bending condition (C) is characterized by an axial load (P) equal to zero and a bending-moment value lower than the balanced one. In such a case, the steel in tension is considered to have yielded ($\varepsilon_s = \varepsilon_{sy}$), whereas the deformation in the compressed steel and the concrete top-edge is obtained through congruence. Then, all the internal forces can be conveniently computed, and the neutral axis depth (x_C) is derived by assuming P = 0 in Equation (7). Then, the ultimate value of the bending moment (M) is derived from Equation (8), after checking the deformation congruence.

Pure tension failure (condition D) is realized under pure tensile load for which all materials reach their tensile strength. When the steel reinforcement yields, the HPFRC jacket gives its traction contribution whereas the inner concrete core is completely neglected (as is commonly assumed at the ultimate limit state for traditional RC structures). No bending action acts on the cross-section by definition and the axial load capacity (P_D) is given by Equation (9):

$$P_D = f_s A_{s,uc} + f_t A_c \quad (9)$$

It is worth noting that the P-M analytical derivation described above is based on classical considerations about the failure modes of concrete, specifically referred to the attainment of the maximum compression capacity in either the HPFRC jacket or inner concrete. However, based on the experimental outcomes, we also propose a different and simplified analytical derivation in order to take into account the reduction of compressive strength in the HPFRC jacket due to the mechanism highlighted in Figure 13. For this scope, in the following discussion, we firstly compare the classical P-M model with the experimental results obtained. Then, the major improvements of the model are presented, and a new comparison is performed.

Figure 18a shows the comparison between the P-M envelope, obtained by applying the classical analytical procedure to the tested column prototype described in Section 2.1, and the experimental results recorded for the specimens S1, S2, and S3. The resulting analytical P-M envelope gives an adequate prediction of the ultimate capacity of the specimen S3, with a slight overestimation in terms of the ultimate moment (M) equal to 4%. Conversely, as expected, for the specimens S1 and S2, a critical not-conservative estimate of the experimental values is obtained. In fact, under the compression-governed stress states, the HPFRC jacket is affected by the detrimental effect of the transverse stress generated by the inner concrete core dilatation (see Section 3.3 for a detailed discussion). This effect is not considered by the adopted classical calculation model even if it is able to strongly reduce the jacket's compressive strength capacity. The magnitude of such a reduction is phenomenologically related to the level of compression acting on the jacketed cross-section, i.e., the neutral axis depth and axial load value, as well as on the thickness and mechanical properties of the HPFRC employed. Since no robust and comprehensive enough experimental results are available, within the proposed calculation procedure, such a reduction effect is accounted for in a simplified and indirect manner by introducing a numerical coefficient (β), which reduces the effectiveness of the HPFRC jacket. β ranges from 0.6 to 1 depending on the neutral-axis position. The minimum value of β is assumed if the neutral-axis is between infinity (pure compression loading condition) and the cross-

section depth (H), whereas β is equal to 1 if the neutral-axis crosses the cross-section above the centerline. Accordingly, Equation (5) is modified as shown in Equation (10), wherein A = B·H and β is assumed to be equal to 0.6, whereas the remaining formulations are not changed since β is equal to one:

$$P_A = f_{u,c}(A_{u,c} - A_{s,uc}) + f_c(\beta A - A_{u,c}) + A_{s,uc}f_s \quad (10)$$

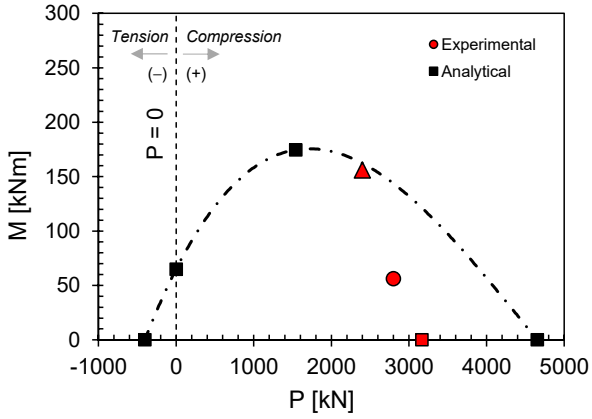

(**a**)

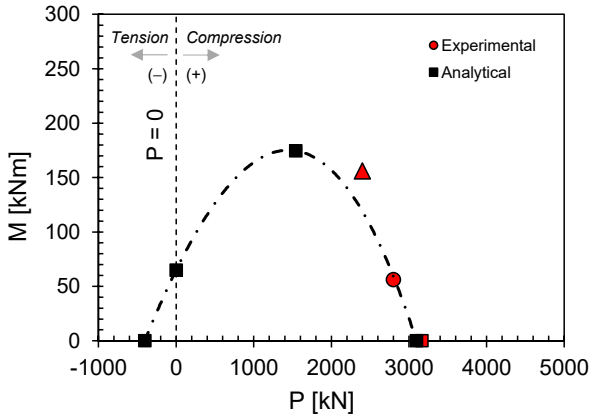

(**b**)

Figure 18. Comparison of experimental axial force-bending (P, M) capacity values and analytical envelopes in which the pure compression point is computed through Equation (5) (**a**) and Equation (10) (**b**).

The P-M envelope obtained by applying Equation (10) is shown in Figure 18b. In this case, the experimental capacity P-M values are predicted with negligible approximation for the specimens S2 and S3, lower than 2%, whereas a conservative prediction is obtained for the specimen S3. This result indicates the importance of investigating the failure mechanisms in the combination of HPFRC and normal (existing) reinforced concrete. Within the limitation of the experimental cases investigated, the available modeling strategies for determining the strength capacity of the jacketed column appear limited, especially for high compression load levels. The use of a reduction factor related to the extent or intensity of the compression acting on the resisting jacketed cross-section might represent a useful tool to incorporate the detrimental effect of the inner concrete core that dilatates at large compressive strains. However, more in-depth experimental investigations are needed to determine the dependency of such a factor from different loading conditions.

5. Conclusions

In this study, a novel strengthening technique applied to existing RC columns was investigated. The technique employs an external jacketing layer made of HPFRC that replaces the existing concrete cover and increases the overall dimensions of the existing column section. The experimental program was carried out on four 1:2 reduced-scale RC column prototypes under a combined axial load and bending uncoupled from shear.

Experimental force–displacement records revealed that the addition of a steel fiber-reinforced jacket to the concrete base material improved the capacity with respect to the benchmark (unreinforced case) expressed as the strengthened-to-non-strengthened ratio, which reached 4.4, 4.8, and 6.5, respectively, for pure compression, low, and large eccentricity cases. No slip between the two components (i.e., plain concrete core and fiber-reinforced jacket) was detected as confirmed by thermographic analyses and the inspection of representative pieces removed from the specimens after the test execution.

Nevertheless, the recorded ultimate values of the axial load and bending moment were lower than the theoretically predicted ones. Such a finding was due to the increase of the detrimental transverse stress state on the HPFRC jacket causing a reduction of its performance, as reflected by local deformation measures.

Due to the lack of specific technical guidance dealing with the design of HPFRC jacketing of existing concrete members, a practice-oriented analytical calculation procedure that aims to compute the axial load–bending moment capacity envelopes was proposed. The analytical calculation required a further refinement in order to properly take into account the interaction between the external high-strength jacket and inner low-strength concrete. Accordingly, the reduction factor proposed was able to take into account the reduction of the performance under high compressive load levels.

The experimental outcomes provided a preliminary set of useful data for better orientation of ongoing research activities. Indeed, the proposed analytical procedure represents a basis for the design of retrofitting of existing RC columns using HPFRC jacketing, although more detailed and comprehensive investigations are necessary to guarantee robust results. In particular, a larger sample set is desired to consider other sources of variability, such as jacketing geometrical parameters (e.g., thickness, properties, and anchorage) and mixed loading cases.

Author Contributions: Conceptualization, C.M. and D.A.; methodology, C.M.; validation, C.M., D.A. and A.O.; formal analysis, P.C.; investigation, P.C.; resources, D.A. and A.O.; data curation, P.C. and C.M.; writing—original draft preparation, P.C.; writing—review and editing, P.C. and C.M.; visualization, P.C.; supervision, D.A. and A.O. All authors have read and agreed to the published version of the manuscript.

Funding: This research received no external funding.

Institutional Review Board Statement: Not applicable.

Informed Consent Statement: Not applicable.

Acknowledgments: The authors kindly acknowledge Global Product Innovation department of Heidelberg Cement Group for material supply and the technical support.

Conflicts of Interest: The authors declare no conflict of interest. The funders had no role in the design of the study; in the collection, analyses, or interpretation of data; in the writing of the manuscript, or in the decision to publish the results.

References

1. Lynn, A.C.; Moehle, J.P.; Mahin, S.A.; Holmes, W.T. Seismic evaluation of existing reinforced concrete building columns. *Earthq. Spectra* **1996**, *12*, 715–739. [CrossRef]
2. Di Ludovico, M.; Verderame, G.M.; Prota, A.; Manfredi, G.; Cosenza, E. Cyclic Behavior of Nonconforming Full-Scale RC Columns. *J. Struct. Eng.* **2014**, *140*, 04013107. [CrossRef]
3. Liu, C.; Fang, D.; Zhao, L. Reflection on earthquake damage of buildings in 2015 Nepal earthquake and seismic measures for post-earthquake reconstruction. *Structures* **2021**, *30*, 647–658. [CrossRef]

4. Ma, Y.; Gong, J.-X. Probability Identification of Seismic Failure Modes of Reinforced Concrete Columns based on Experimental Observations. *J. Earthq. Eng.* **2017**, *22*, 1881–1899. [CrossRef]
5. Fardis, M.N. *Seismic Design, Assessment and Retrofitting of Concrete Buildings: Based on EN-Eurocode 8*; Springer: Amsterdam, The Netherlands, 2009.
6. Cassese, P.; De Risi, M.T.; Verderame, G.M. A modelling approach for existing shear-critical RC bridge piers with hollow rectangular cross section under lateral loads. *Bull. Earthq. Eng.* **2018**, *17*, 237–270. [CrossRef]
7. Masi, A.; Vona, M. Estimation of the in-situ concrete strength: Provisions of the European and Italian seismic codes and possible improvements. In *Proceedings of the Eurocode 8 Perspectives from the Italian Standpoint Workshop, Napoli, Italy, January 2009*; Naples, E., Ed.; Doppiavoce: Napoli, Italy, 2009.
8. Ma, Y.; Che, Y.; Gong, J. Behavior of corrosion damaged circular reinforced concrete columns under cyclic loading. *Constr. Build. Mater.* **2012**, *29*, 548–556. [CrossRef]
9. Priestley, M.J.N.; Seible, F.; Calvi, G.M. *Seismic Design and Retrofit of Bridges*; John Wiley & Sons, Inc.: New York, NY, USA, 1996.
10. Campione, G.; Fossetti, M.; Giacchino, C.; Minafò, G. RC columns externally strengthened with RC jackets. *Mater. Struct.* **2013**, *47*, 1715–1728. [CrossRef]
11. Belal, M.F.; Mohamed, H.M.; Morad, S.A. Behavior of reinforced concrete columns strengthened by steel jacket. *HBRC J.* **2015**, *11*, 201–212. [CrossRef]
12. Teng, J.G.; Chen, J.F.; Smith, S.; Lam, L. Behaviour and strength of FRP-strengthened RC structures: A state-of-the-art review. *Proc. Inst. Civ. Eng. Struct. Build.* **2003**, *156*, 51–62. [CrossRef]
13. Lignola, G.P.; Prota, A.; Manfredi, G.; Cosenza, E. Experimental Performance of RC Hollow Columns Confined with CFRP. *J. Compos. Constr.* **2007**, *11*, 42–49. [CrossRef]
14. Han, Q.; Wen, J.; Du, X.; Jia, J. Experimental and numerical studies on seismic behavior of hollow bridge columns retrofitted with carbon fiber reinforced polymer. *J. Reinf. Plast. Compos.* **2014**, *33*, 2214–2227. [CrossRef]
15. Shannag, M.J.; Barakat, S.; Abdul-Kareem, M. Cyclic behavior of HPFRC-repaired reinforced concrete interior beam-column joints. *Mater. Struct.* **2002**, *35*, 348–356. [CrossRef]
16. Meda, A.; Plizzari, G.A.; Rinaldi, Z.; Martinola, G. Strengthening of R/C existing columns with high performance fiber rein-forced concrete jacket. In Proceedings of the Concrete Repair, Rehabilitation and Retrofitting II, 2nd International Conference on Concrete Repair, Rehabilitation and Retrofitting, ICCRRR-2, Cape Town, South Africa, 24–26 November 2008; CRC Press: Boca Raton, FL, USA; pp. 461–462.
17. Martinola, G.; Meda, A.; Plizzari, G.; Rinaldi, Z. Strengthening and repair of RC beams with fiber reinforced concrete. *Cem. Concr. Compos.* **2010**, *32*, 731–739. [CrossRef]
18. Beschi, C.; Meda, A.; Riva, P. Column and Joint Retrofitting with High Performance Fiber Reinforced Concrete Jacketing. *J. Earthq. Eng.* **2011**, *15*, 989–1014. [CrossRef]
19. Beschi, C.; Riva, P.; Metelli, G.; Meda, A. HPFRC Jacketing of Non Seismically Detailed RC Corner Joints. *J. Earthq. Eng.* **2014**, *19*, 25–47. [CrossRef]
20. Del Zoppo, M.; Menna, C.; Di Ludovico, M.; Asprone, D.; Prota, A. Opportunities of light jacketing with Fibre Reinforced Cementitious Composites for seismic retrofitting of existing RC columns. *Compos. Struct.* **2021**, *263*, 113717. [CrossRef]
21. Naaman, A.E. High performance fiber reinforced cement composites: Classification and applications. In Proceedings of the CBM-CI International Workshop, Karachi, Pakistan, 10–11 December 2007; pp. 389–401.
22. Li, V.; Stang, H.; Krenchel, H. Micromechanics of crack bridging in fibre-reinforced concrete. *Mater. Struct.* **1993**, *26*, 486–494. [CrossRef]
23. Singh, H. *Steel Fiber Reinforced Concrete: Behavior, Modelling and Design*; Springer: Singapore, 2016.
24. Feo, L.; Ascione, F.; Penna, R.; Lau, D.; Lamberti, M. An experimental investigation on freezing and thawing durability of high performance fiber reinforced concrete (HPFRC). *Compos. Struct.* **2020**, *234*, 111673. [CrossRef]
25. Shannag, M.J.; Abu-Dyya, N.; Abu-Farsakh, G. Lateral load response of high performance fiber reinforced concrete beam–column joints. *Constr. Build. Mater.* **2005**, *19*, 500–508. [CrossRef]
26. Cho, C.-G.; Kim, Y.-Y.; Feo, L.; Hui, D. Cyclic responses of reinforced concrete composite columns strengthened in the plastic hinge region by HPFRC mortar. *Compos. Struct.* **2012**, *94*, 2246–2253. [CrossRef]
27. Koo, I.Y.; Hong, S.G. Strengthening RC columns with ultra high performance concrete. In Proceedings of the 2016 Structures Congress (Strctures16), Jeju Island, Korea, 28 August–1 September 2016.
28. Meda, A.; Mostosi, S.; Rinaldi, Z.; Riva, P. Corroded RC columns repair and strengthening with high performance fiber reinforced concrete jacket. *Mater. Struct.* **2015**, *49*, 1967–1978. [CrossRef]
29. Di Carlo, F.; Meda, A.; Rinaldi, Z. Numerical cyclic behaviour of un-corroded and corroded RC columns reinforced with HPFRC jacket. *Compos. Struct.* **2017**, *163*, 432–443. [CrossRef]
30. Sadouki, H.; Denarié, E.; Brühwiler, E. Validation of a FEA model of structural response of RC-cantilever beams strengthened with a (R-) UHPFRC layer. *Constr. Build. Mater.* **2017**, *140*, 100–108. [CrossRef]
31. Sakr, M.A.; El-Khoriby, S.R.; Khalifa, T.M.; Nagib, M.T. Modeling of RC shear walls strengthened with ultra-high performance fiber reinforced concrete (UHPFRC) jackets. *Eng. Struct.* **2019**, *200*, 109696. [CrossRef]
32. Sakr, M.A.; El Korany, T.M.; Osama, B. Analysis of RC columns strengthened with ultra-high performance fiber reinforced concrete jackets under eccentric loading. *Eng. Struct.* **2020**, *220*, 111016. [CrossRef]

33. *2005 European Standard EN 1992-1-1, Eurocode 2, Design of Concrete Structures. Part 1–1: General Rules and Rules for Buildings*; CEN: Brussels, Belgium, 2004.
34. *EN 1998-1-1 Eurocode 8: Earthquake Resistant Design of Structures—Part 1: General Rules and Rules for Buildings*; CEN: Brussels, Belgium, 2004.
35. ACI Committee 318. *Building Code Requirements for Structural Concrete and Commentary (ACI CODE 318-19)*; American Concrete Institute: Indianapolis, IN, USA, 2019.
36. American Society of Civil Engineers. *Seismic Evaluation and Retrofit of Existing Buildings (Standard ASCE/SEI 41-17)*; American Society of Civil Engineers: Reston, VA, USA, 2017.
37. D.M. 17/01/2018. Norme Tecniche per le Costruzioni (NTC 2018); Gazzetta Ufficiale, Serie Generale n. 42 del 20/02/2018, Supplemento Ordinario n.8; Roma, Italy. 2018. Available online: https://biblus.acca.it/download/norme-tecniche-per-le-costruzioni-2018-ntc-2018-pdf/ (accessed on 1 November 2021). (In Italian).
38. CNR-DT 204-2006. *Istruzioni per la Progettazione, l'Esecuzione ed il Controllo di Strutture di Calcestruzzo Fibrorinforzato*; Consiglio Nazionale delle Ricerche: Roma, Italy, 2007. (In Italian)
39. International Federation for Structural Concrete. *Fib Model Code for Concrete Structures 2010*; Ernst & Sohn: Berlin, Germany, 2013. [CrossRef]
40. Verderame, G.; Polese, M.; Mariniello, C.; Manfredi, G. A simulated design procedure for the assessment of seismic capacity of existing reinforced concrete buildings. *Adv. Eng. Softw.* **2010**, *41*, 323–335. [CrossRef]
41. Ohtaki, T. An experimental study on scale effects in shear failure of reinforced concrete columns. *Strain* **2000**, *500*, 36–D13.
42. Mariniello, C. Una Procedura Meccanica nella Valutazione della Vulnerabilità Sismica di Edifici in c.a. Ph.D. Thesis, University of Naples Federico II, Naples, Italy, 2008.
43. *EN 12390-3:2019, Testing Hardened Concrete–Part 3: Compressive Strength of Test Specimens*; European Committee for Standardization: Brussels, Belgium, 2019.
44. Wille, K.; El-Tawil, S.; Naaman, A. Properties of strain hardening ultra high performance fiber reinforced concrete (UHP-FRC) under direct tensile loading. *Cem. Concr. Compos.* **2014**, *48*, 53–66. [CrossRef]
45. Cassese, P.; De Risi, M.T.; Verderame, G.M. Seismic Assessment of Existing Hollow Circular Reinforced Concrete Bridge Piers. *J. Earthq. Eng.* **2020**, *24*, 1566–1601. [CrossRef]
46. *EN ISO 15630-1:2019, Steel for the Reinforcement and Prestressing of Concrete–Test Methods–Part 1: Reinforcing Bars, Wire Rod and Wire (ISO 15630-1:2010)*; European Committee for Standardization: Brussels, Belgium, 2019.
47. Chandrasekaran, S.; Nunziante, L.; Serino, G.; Carannante, F. Axial Force-Bending Moment Limit Domain and Flow Rule for Reinforced Concrete Elements Using Euro Code. *Int. J. Damage Mech.* **2009**, *19*, 523–558. [CrossRef]
48. Júlio, E.N.; Branco, F.; Silva, V.D. Concrete-to-concrete bond strength. Influence of the roughness of the substrate surface. *Constr. Build. Mater.* **2004**, *18*, 675–681. [CrossRef]
49. Minafò, G.; Di Trapani, F.; Amato, G. Strength and ductility of RC jacketed columns: A simplified analytical method. *Eng. Struct.* **2016**, *122*, 184–195. [CrossRef]
50. Maalej, M.; Li, V. Flexural Strength of Fiber Cementitious Composites. *J. Mater. Civ. Eng.* **1994**, *6*, 390–406. [CrossRef]
51. Barros, J.; Cunha, V.M.C.F.; Ribeiro, A.F.; Antunes, J.A.B. Post-cracking behaviour of steel fibre reinforced concrete. *Mater. Struct.* **2005**, *38*, 47–56. [CrossRef]
52. Chalioris, C. Analytical approach for the evaluation of minimum fibre factor required for steel fibrous concrete beams under combined shear and flexure. *Constr. Build. Mater.* **2013**, *43*, 317–336. [CrossRef]
53. Singh, H. Flexural modelling of steel-fibre-reinforced concrete member with conventional tensile rebars. *Proc. Inst. Civ. Eng. Struct. Build.* **2016**, *169*, 54–66. [CrossRef]
54. UNI 11039. *Concrete Reinforced with Steel Fibers; (1a) Part I: Definitions, Classification and Designation; (1b) Part II: Test Method to Determine First Cracking Strength and Ductility Indexes*; UNI Editions: Milan, Italy, 2003. (In Italian)